MODELLING FEW-MODED HORNS FOR FAR-IR SPACE APPLICATIONS.

Ruth Colgan,[1] J.Anthony Murphy,[1] Bruno Maffei,[2] Creidhe O'Sullivan,[1] Richard Wylde[2] and Peter Ade[2].

[1] National University of Ireland Maynooth, Co.Kildare. Ireland
[2] Queen Mary and Westfield College, London E1 4NS, UK.

Abstract:

Few-moded or over-moded horns are now being proposed for far-IR space receiver systems, e.g. the High Frequency Instrument (HFI) on the ESA PLANCK Surveyor. In such systems individual waveguide modes can couple independently to an overmoded detector (such as a bolometer in an integrating cavity). We consider in detail the case of a cylindrically symmetric configuration consisting of a corrugated conical horn connected to waveguide filter also corrugated, such as is proposed for the HFI instrument. Such antenna feeds have the advantage of high coupling efficiency combined with low sidelobe level beam patterns. In the paper we present two alternative techniques for modelling few moded horn antennas. The first is based on a scattering matrix description of propagation in a non-uniform wave-guide structure, while the second approach uses hybrid mode solutions for a waveguide with corrugated walls. We also present computed and experimental data for an example prototype HFI horn.

1. Introduction

Few-moded or over-moded horns are finding application in far-IR detector systems where high efficiency is required with the low sidelobe response pattern associated with single mode operation. Using standard techniques borrowed from antenna engineering it is possible to model such partially coherent *multi-moded* horns in a straightforward way [1,2]. We assume that the horn is connected to an integrating cavity containing a black-body source/detector via a wave-guide filter which limits the number of modes that can propagate (see Fig.1). This is best achieved by the use of a flared section at the back of the waveguide, which is then coupled without an impedance mismatch to an integrating cavity. In this configuration the black-body detector/source independently (incoherently) couples to the individual spatially coherent modes of the wave-guide at the cavity end. Only non-evanescent modes propagate through the filter, of course, and there will be scattering of power between modes if the wave-guide is not of uniform cross section (as for example if the guide is corrugated). The calculation of the radiation pattern (including diffraction effects) then amounts to summing the far-field radiation pattern of each non-evanescent mode at the cavity end of the horn/waveguide structure.

The scattering matrix description of non-uniform wave-guides based on mode matching is a powerful computational method and can be used to predict the beam patterns of corrugated horn antenna feeds. The technique is especially useful if the number of corrugations per wavelength is not very large, as then the surface impedance hybrid-mode description referred to below may become unreliable [3]. In the mode matching approach the profile of the waveguide plus horn is replaced by a series of uniform waveguide segments, and the longitudinal cross section can then be viewed as a series of steps. The technique involves matching the total electric and magnetic fields at each junction between the uniform segments so that conservation of complex power is maintained. The technique is discussed in detail by Olver et al [4].

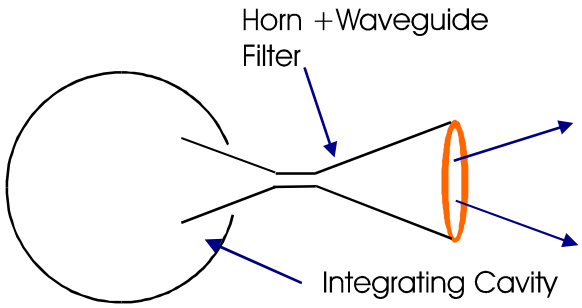

Figure 1. Corrugated horn and waveguide filter feeding an integrating cavity

The surface impedance model can also be used in predicting the radiation pattern of a corrugated horn and waveguide in the limit of many corrugations per wavelength. The waveguide is considered as having a surface defined by the edges of the corrugations with different impedances in the axial and transverse directions [3]. The true modes of propagation of such a system cannot be pure TE or TM, but rather a hybrid combination that depends on the depths of the corrugations and the radius (width) of the guide. The application of the boundary conditions leads to the modal propagation coefficients and transverse wavenumbers of a complete set of such hybrid modes. The surface-impedance method is simple and quite accurate and is particularly useful in the design of the wave-guide filter section. However, when the waveguide radius is of order one wavelength, space harmonics must be included if an accurate cross-polar pattern is to be modelled [3].

2. Mode Matching Approach to Multi-moded Horns

The mode scattering properties of the system as a whole or any section of it can be represented by a single scattering matrix *S*. The reflection and transmission characteristics are determined by the usual equation (see for example Olver 1994 [4]):

$$\begin{bmatrix} B \\ D \end{bmatrix} = [S]\begin{bmatrix} A \\ C \end{bmatrix} = \begin{bmatrix} S_{11} & S_{12} \\ S_{21} & S_{22} \end{bmatrix}\begin{bmatrix} A \\ C \end{bmatrix},$$

where A and B are vectors containing the forward and reflected mode coefficients, respectively, looking into the system at the input side, and C and D are vectors of the incident and transmitted mode coefficients, respectively, looking into the system at the output plane. We now summarize the derivation of the S scattering matrix for a cylindrically symmetric waveguide structure (corrugated or smooth walled).

For cylindrical waveguides the transverse electric fields of the corresponding two orthogonal sets of TE modes and two sets of TM modes are:

$$\begin{pmatrix} \mathbf{e}_{nl}^{TE,c} \\ \mathbf{e}_{nl}^{TE,s} \end{pmatrix} = \sqrt{\frac{(2-\delta_{n0})}{\pi a^2 J_{n+1}^2(p_{nl})}}\left[J_n'(p_{nl}r/a)\begin{pmatrix} \cos n\phi \\ \sin n\phi \end{pmatrix}\mathbf{r} + \frac{nJ_n(q_{nl}r/a)}{q_{nl}r/a}\begin{pmatrix} -\sin n\phi \\ \cos n\phi \end{pmatrix}\phi \right]$$

$$\begin{pmatrix} \mathbf{e}_{nl}^{TM,c} \\ \mathbf{e}_{nl}^{TM,s} \end{pmatrix} = \sqrt{\frac{(2-\delta_{n0})}{\pi a^2 (1-(n/q_{nl})^2) J_n^2(q_{nl})}}\left[\frac{nJ_n(q_{nl}r/a)}{q_{nl}r/a}\begin{pmatrix} \cos n\phi \\ -\sin n\phi \end{pmatrix}\mathbf{r} - J_n'(q_{nl}r/a)\begin{pmatrix} \sin n\phi \\ \cos n\phi \end{pmatrix}\phi \right],$$

where p_{nl} represents the *lth* zero of $J_n(z)$, and q_{nl} represents the *lth* zero of $dJ_n/dz\,(z)$ [5]. The constant of proportionality has been chosen to make $\int_A |\mathbf{e}_l^{te/tm}|^2\, rdrd\phi$ equal to unity. The two possible orthogonal modes for each value of n and l arise from the choice of the z component of the appropriate field being either proportional to $\cos(n\phi)$ or $\sin(n\phi)$. On ordering the guide modes by their cutoff wavelength (so that those of odd order are TE while those of even order are TM) any coherent field propagating within the waveguide filter and horn can be represented by:

$$\mathbf{e}_{total} = \sum_{nl} \alpha_{nl}^c \mathbf{e}_{nl}^{TE,c} + \alpha_{nl}^s \mathbf{e}_{nl}^{TE,s} + \beta_{nl}^c \mathbf{e}_{nl}^{TM,c} + \beta_{nl}^s \mathbf{e}_{nl}^{TM,s} = \sum_{ni} A_{ni}^c \mathbf{e}_{ni}^{G,c} + A_{ni}^s \mathbf{e}_{ni}^{G,s},$$

where: $\mathbf{e}_{n,2l-1}^G = \mathbf{e}_{n,l}^{TE}$, $\mathbf{e}_{n,2l}^G = \mathbf{e}_{n,l}^{TM}$, and it is understood that the summation is also over both orthogonal mode sets.

Because of the cylindrical symmetry of the junction discontinuity, in propagating through the waveguide and horn only scattering between modes of the same azimuthal index and same z-component dependance on cos/sin($n\phi$) is possible. It is therefore convenient to compute the overall scattering matrix $S^{(n)}$ for each azimuthal order separately. First it is necessary to divide the overall waveguide/horn structure into a series of segments with a step discontunuity occuring at the beginning and end of each section. At a step disconituity where the guide radius increases from a to b the submatrix elements of the scattering matrix $S^{(n)}$ can be written as:

$$S_{11} = (R^* + P^+ Q^{-1} P)^{-1}(R^* - P^+ Q^{-1} P) \qquad S_{12} = 2(R^* + P^+ Q^{-1} P)^{-1} P^+$$
$$S_{21} = 2(Q + P(R^*)^{-1} P^+)^{-1} P \qquad S_{22} = -(Q + P(R^*)^{-1} P^+)^{-1}(Q - P(R^*)^{-1} P^+)$$

where for both the TE and TM modes defined above $R_{ij} = (1/Z_{nl}^{TE/TM})^* \delta_{ij}$, and $Q_{ij} = (1/Z_{nl}^{TE/TM})^* \delta_{ij}$ and cross coupled powers $P_{ij} = \int_0^a \mathbf{e}_{nl}^a \times (\mathbf{h}_{nl'}^b)^* dA$, with appropriate values for the guide impedance Z [5], and i and j determined by the ordering of the TE/TM modes. Note the equations here differ slightly from those presented in Olver [4]. The superscripts a and b on the **e** and **h** fields indicates the appropriate guide radius for the mode. The P_{ij} can be evaluated from the following expressions for the cross coupled power between the modes on either side of the discontinuity:

$$P_{TE->TE} = -\frac{\pi(1+\delta_{n0})\, D_{nl}(a) D_{nl'}(b) q_{nl} J_n(q_{nl}) J_n'(q_{nl'} a/b)}{[(q_{nl'}/b)^2 - (q_{nl}/a)^2](Z_{TE}^b)^*},$$

$$P_{TM->TM} = \frac{\pi(1+\delta_{n0})\, C_{nl}(a) C_{nl'}(b) p_{nl'} a/b\, J_n'(p_{nl}) J_n(p_{nl'} a/b)}{[(p_{nl'}/b)^2 - (p_{nl}/a)^2](Z_{TM}^b)^*},$$

$$P_{TE->TM} = \frac{\pi abn D_{nl}(a) C_{nl'}(b)\, J_n(p_{nl'} a/b) J_n(q_{nl'})}{[p_{nl'} q_{nl}](Z_{TM}^b)^*} \quad \text{and} \quad P_{TM->TE} = 0$$

where $C_{nl}(a) = \sqrt{\dfrac{(2-\delta_{n0})}{\pi a^2 J_{n+1}^2(p_{nl})}}$ and $D_{nl}(b) = \sqrt{\dfrac{(2-\delta_{n0})}{\pi a^2 (1-(n/q_{nl})^2) J_n^2(q_{nl})}}$

For a step in which $a > b$ then S_{11} (a>b) = S_{22} (a<b), S_{12} (a>b) = S_{21} (a<b), S_{21} (a>b) = S_{12} (a<b), and S_{22} (a>b) = S_{11} (a<b). The propagation of the mode along the waveguide sections can also be described in terms of propagation "scattering" matrices. For a given azimuthal order the overall scattering matrix for the horn and waveguide can be derived by cascading the scattering matrices for the sections in the appropriate way [4]. At the end of the horn the fields are launched into free space. There is a sudden jump in the impedance and there may be significant reflections at that point. We can model this effect to a good approximation by assuming the horn aperture lies in an infinite ground plane. This in turn can be modelled by a very large step into a waveguide of infinite diameter. Finite element analysis can be applied to the real horn aperture configuration, if low level sidelobe effects are important.

The modes at the horn aperture then propagate without scattering to the far-field. In the example multi-moded horns we have chosen to analyse all of the waveguide

modes at the entrance to the waveguide section are assumed to be equally excited. The far field pattern for the horn plus waveguide and flare is then given by:

$$I \propto \sum_{nj} \left(\left| \sum_i [S_{21}^n]_{ij} \, \mathbf{e}_{ni}^{ff\,c} \right|^2 + \left| \sum_i [S_{21}^n]_{ij} \, \mathbf{e}_{ni}^{ff\,s} \right|^2 \right),$$

where *c* and *s* refer to the two possible orthogonal modes for a given *ni*. The beam patterns on the sky correspond to the field patterns produced after scattering by the individual modes *at the cavity entrance* to the waveguide/horn structure added in quadrature. Note in the above sum the subscripts *n* refers to the azimuthal order of the mode, and for *i* and *j* odd or even the modes are TE or TM, respectively. The results of modelling the beam pattern performance of one of the prototype horns for the HFI on the PLANCK Surveyor using the mode-matching approach is discussed in section 4.

3. Surface Impedance Model.

A corrugated horn or waveguide is considered as having a surface defined by the edges of the corrugations with different impedances in the axial and transverse directions [3]. The characteristics of the true hybrid TE/TM modes of propagation depend on the depths of the corrugations and the radius (width) of the guide. The fundamental mode in a very wide cylindrical waveguide with corrugation depths of $\lambda/4$ is the balanced hybrid HE_{11} mode used in predicting the radiation patterns of single moded corrugated horns. In a multi-moded horn we will still obtain higher order balanced hybrid modes, where such modes all have zero transverse fields at the horn aperture edge. The effective impedance for any currents flowing across the corrugations is infinite, so that H_ϕ is zero and E_ϕ is also zero if there are many corrugations per wavelength. Consequently, such horns will produce beam patterns with low sidelobe levels because of the gradually tapered fields at the horn aperture. Away from the balanced hybrid condition higher sidelobe levels are to be expected as the effective surface impedance across the corrugations is no longer infinite. This may be an issue for the design of broadband horn feed systems.

In the throat of a horn the effective impedance produced by the corrugations becomes mode dependent and is also non-infinite even for slot depths of $\lambda/4$. However, it is not necessary to maintain the balanced mode condition in the waveguide at the back of the horn as long as one knows the propagation characteristics. The critical issue for a few-moded horn is the mode filtering properties of this waveguide section. In order to determine which modes can propagate in a corrugated waveguide it is necessary to solve the characteristic equation for the propagation coefficient β (i.e. the guide wavenumber). In this approach the waveguide is regarded as consisting of an inner region of radius r_1 bounded by an impedance surface determined by the corrugation

slot depth. For this to be valid there must be a sufficient number of corrugations per wavelength so that they effectively mimic a continuous surface. It is assumed that the slots are narrow and only a single non-propagating TM mode is capable of existing in the slots.

Matching the admittance of the *m*th order TM mode in the slot with that of the mode in the inner region of the guide yields the characteristic equation for β [3]:

$$F_m(Kr_1) - \frac{(m\beta/k)^2}{F_m(Kr_1)} = \left(\frac{Kr_1}{kr_1}\right)^2 S_m(kr_1, kr_0)\,,$$

where $K^2 + \beta^2 = k^2$, r_o is the radius to the bottom of the corrugation and $S_m(x, y)$ is given by the equation:

$$S_m(x,y) = x\,\frac{J_m'(x)Y_m(y) - J_m(y)Y_m'(x)}{J_m(x)Y_m(y) - J_m(y)Y_m(x)}\,.$$

For the hybrid modes the *z* components of the electric and magnetic fields for the two possible orthogonal modes are defined to be:

$$E_z(r,\phi) = a_m J_m(Kr)\begin{pmatrix}\cos m\phi\\ \sin m\phi\end{pmatrix} \qquad \text{and} \qquad H_z(r,\phi) = a_m y_0 \Lambda J_m(Kr)\begin{pmatrix}\sin m\phi\\ \cos m\phi\end{pmatrix},$$

where y_0 is the admittance of free space. The transverse fields can be derived from the *z*-component of the fields [5]. The requirement that the ϕ component of the electric field be zero at the corrugations yields the following relationship between Λ and β:

$$\Lambda = -\frac{m\beta/k}{F_m(Kr_1)}\,.$$

The cut-off condition β = 0 yields either $F_m(Kr_1) = 0$, where the mode is pure TE-type in the limit, or $F_m(Kr_1) = S_m(kr_1, kr_0)$, where the mode exhibits pure TM properties in the limit. In the former case the boundary condition corresponds to that of a TE mode in a guide of radius r_1, while the latter corresponds to a TM mode in a uniform waveguide of radius r_0. For fixed values of r_1 and r_0 as the frequency is increased the high frequency cut-off condition is eventually reached where β/k tends to ∞.

Figure 2 shows dispersion curves for modes of azimuthal order 1. As kr_1 increases from the low-frequency cut-off, a balanced-hybrid condition is reached where $\Lambda^2 = 1$. For high frequencies the HE_{11} mode is balanced hybrid when the corrugation depth approaches $\lambda/4$. A fast-wave to slow-wave transition takes place at $k = \beta$ (dashed line). Beyond this, in the slow-wave domain, a high-frequency cut-off eventually occurs where β/k tends to infinity and the mode terminates. Figure 3 shows a plot of the high-frequency cut-off values for the HE_{11} and a selection of other modes.

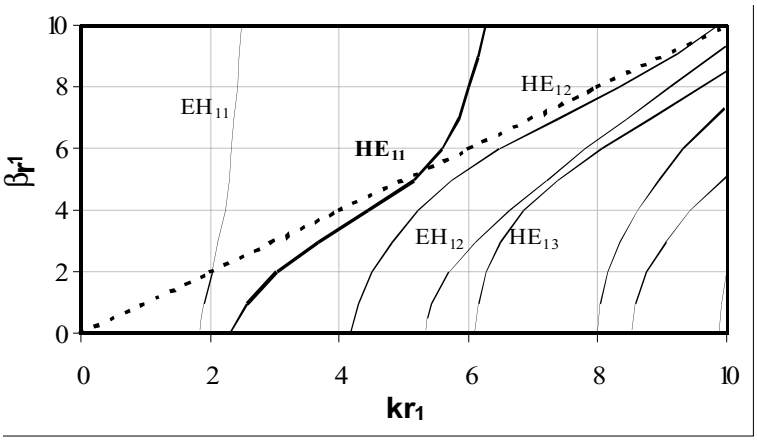

Figure 2. Dispersion characteristics for modes of azimuthal order 1 in a corrugated waveguide with $r_1/r_o = 0.6$.

Charts such as Figure 3 can be used to determine the bandwidth of corrugated guide if certain modes are to be propagated. Within the surface impedance model, a mode is sustained with increasing frequency over the range in which the corrugation depth increases by slightly more than $\lambda/2$.

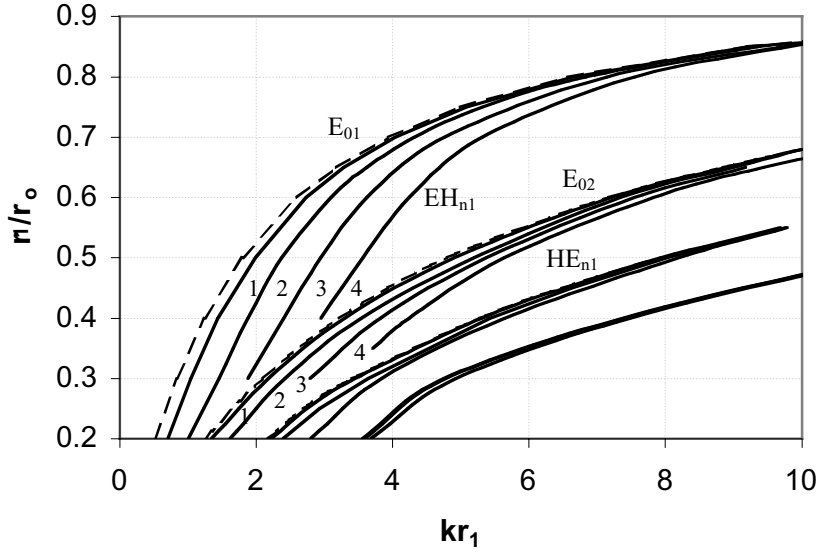

Figure 3. High-frequency cut-off values as a function of wavenumber for different ratios of r_1/r_o. (After Olver [4])

In the case of the high-frequency cut-offs, higher-order space harmonics have a non-negligible effect, and an error, depending on the mode and waveguide parameters, is to be expected for the SI model predictions. Olver [4] shows these to be of the order of 10%.

As the wave-guide flares out into the horn, the value of β, K and Λ all change as is clear from Fig. 2. The x- and y-components of the far field patterns of the nl hybrid modes in the guide can be shown to depend on:

$$e_{x,nl} = (\beta/k + \Lambda) I_{n,l-1}(\sin\theta)\cos(n-1)\phi + (\beta/k - \Lambda) I_{n,l+1}(\sin\theta)\cos(n+1)\phi,$$
$$e_{y,nl} = (\beta/k + \Lambda) I_{n,l-1}(\sin\theta)\sin(n-1)\phi + (\beta/k - \Lambda) I_{n,l+1}(\sin\theta)\sin(n+1)\phi,$$

for the two orthogonal polarisation directions, where $I_{n,l}(\sin\theta)$ represents the integral:

$$I_{n,l}(\sin\theta) = \int_0^a J_n(p_{nl} r/a) J_n(kr\sin\theta)\exp(-ikr^2/2L)\, rdr\,,$$

where a is the radius of the horn aperture, and L is the axial length of the horn. Thus, the corresponding intensity patterns can be shown to be:

$$P_{nl}(\theta) \propto \left[(\beta/k + \Lambda) I_{n,l-1}(\sin\theta)\right]^2 + \left[(\beta/k - \Lambda) I_{n,l+1}(\sin\theta)\right]^2$$

If we assume that the hybrid modes independently couple to the cavity then the overall pattern will be given by: $P(\theta) = \Sigma_{nl} P_{nl}(\theta)$.

4. Experimental Results

Some preliminary results for multi-moded horn operation, both experimental and theoretical are included here for comparison. The test waveguide corrugated structure is one of the prototype HFI back to back conical horns manufactured for the PLANCK Surveyor [7]. The horn/waveguide structure is 92.75 mm in length and has an aperture diameter of 12.43 mm at the output side. The horn was optimised for single mode operation at 150GHz, but also tested in multi-mode operation at 240GHz. The groove depth is thus 0.5 mm at the horn aperture (i.e. quarter wavelength deep at 150GHz), with both a corrugation and groove width of 0.25 mm, (i.e. 4 corrugations per wavelength at 150GHz). In the filter section the waveguide has r_1-r_o = 0.5 mm and r_1/r_o = 0.6. A schematic diagram of this type of horn is shown below Fig. 4.

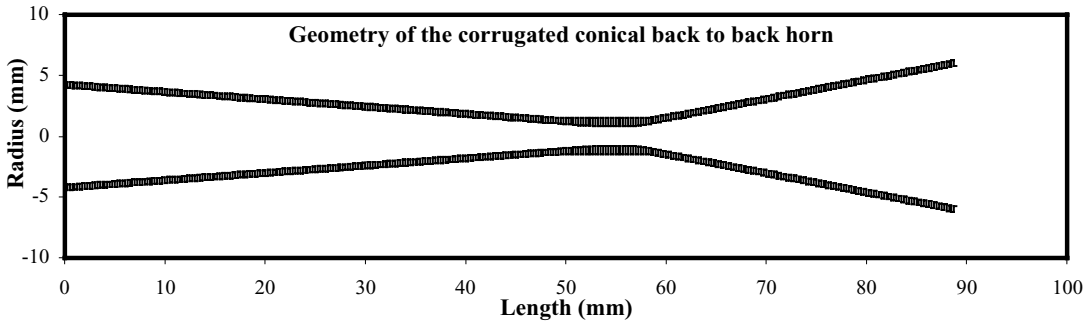

Figure 4. Back-to-back horn configuration.

The experimental FTS spectral transmission measurements of the horn/waveguide are plotted in Figure 5. The high- and low-frequency cut-offs, the fast-wave to slow-wave transition point and the balanced hybrid point for the HE_{11} mode in a waveguide with $r_1/r_o = 0.62$ are also marked. The fall-off in efficiency before the high-frequency cut-off may be due to the fast to slow wave transition increasing the losses in the guide and affecting the on-axis gain of the beam pattern of the horn.

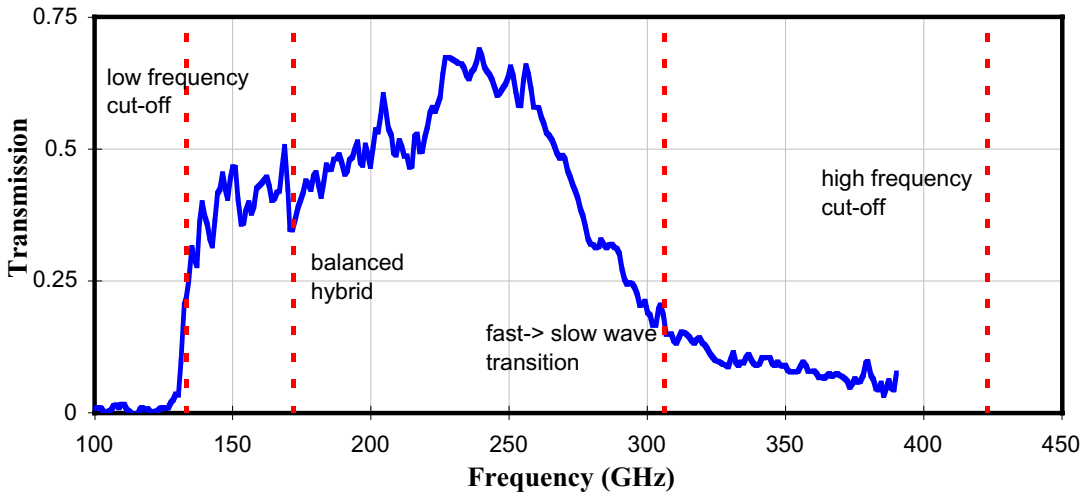

Figure 5. The transmission of a pair of back to back conical corrugated horns joined by a waveguide section with r_1-r_o = 0.5mm and $r_1/r_o = 0.62$ at its narrowest point

Figure 6 shows the comparison of the theoretical mode-matching model with experimental data taken at 150GHz for single mode operation. The source is plane polarized and spatially coherent (a frequency doubler fed by a Gunn oscillator).

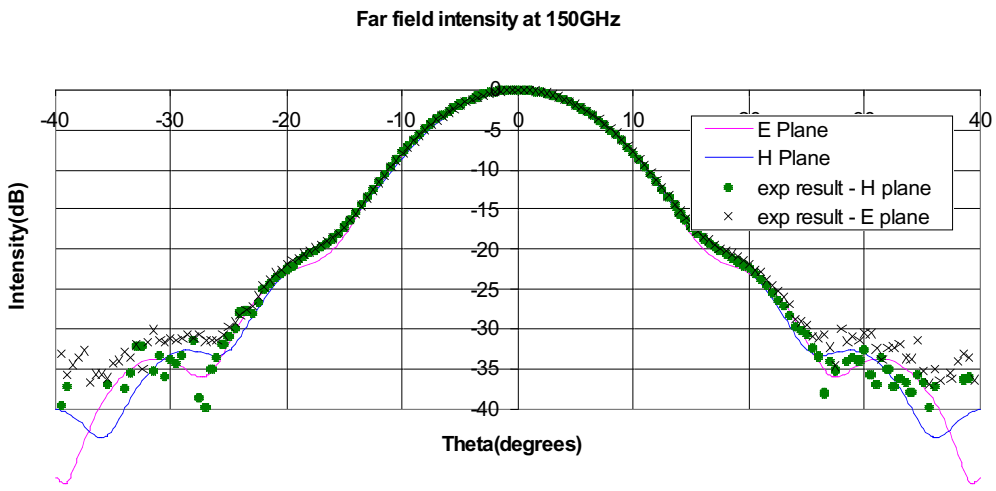

Figure 6. Spot frequency beam patterns for HFI prototype back to back horn at 150 GHz.

Figure 7 shows the broadband experimental measurements for the same horn centred at 240GHz with a 25% bandwidth using an incoherent source (mercury arc blackbody source at 2000 K). At 240 GHz we expect to see multi-mode operation. The experimental data compare well with mode-matching model model predictions, where the broadband numerical data was obtained by running the model at the centre and edges of the band and combining the resulting numerical outputs. The experimental data were taken with the test horn in a dewar, with some resultant vignetting at the dewar window suffered by the beam for angles bigger than 20 degrees.

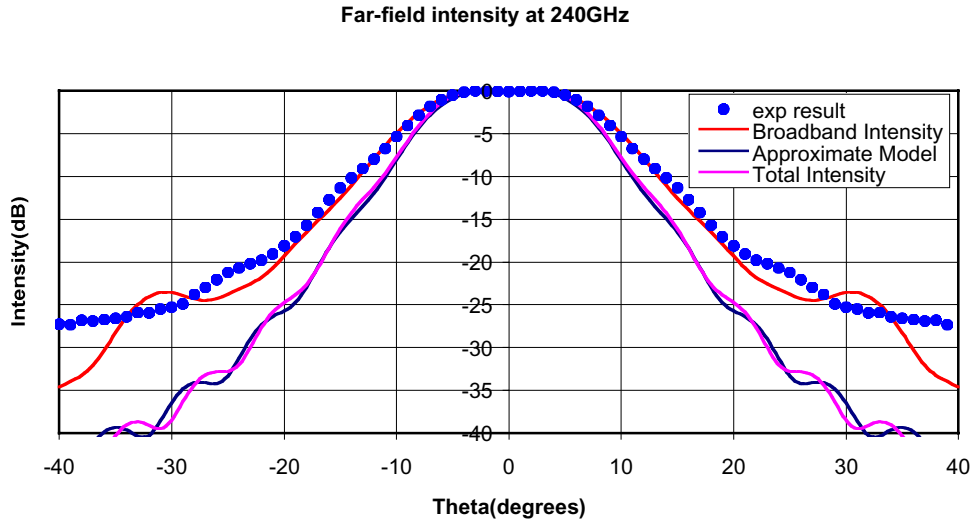

Figure 7. Comparison of experimental data with numerical model results at 240 GHz.

The narrower far-field patterns also shown in Fig. 7 are theoretical beam patterns for the same horn at the centre of the frequency band (i.e. at 240GHz) using both the surface impedance and mode-matching approaches. These results show in this case both approaches are in good agreement with each other. It is found from a hybrid mode viewpoint for a horn with an aperture of 6 mm radius, and corrugations of depth 0.4 λ, that $\beta > 0.99\ k$, with K = 3.7103, 2.35339 and 3.74811, and that Λ = 0, 1.133 and 1.170, for the H_{01}, HE_{11} and HE_{21} modes, respectively. In this case the modes are not pure balanced modes (which require Λ = +1 for HE modes), although they are close to meeting the condition. Thus, at least in this example, the depths of the corrugations are not very critical in terms of causing a deterioration in the low sidelobe levels.

5. Conclusions

In this paper we have discussed two different approaches to modelling corrugated horn-filter configurations. These types of horns are planned for use as incoherent detector feeds for bolometric detector systems on forthcoming space missions. Good agreement with experimental measurement performed on a prototype horn antenna for the HFI instrument was recorded.

Acknowledgements

The authors would like to acknowledge the support of Enterprise Ireland in this research programme.

References

1. J.A. Murphy and R. Padman, "Radiation patterns of few moded horns and condensing lightpipes," *Infrared Physics*, **31**, 291, 1991.
2. R. Padman and J.A. Murphy, "Radiation Patterns of scalar horns," *Infrared Physics*, **31**, 441, 1991.
3. P.J.B. Clarricoats and A.D. Olver, *Corrugated Horns for Microwave Antennas,* Peter Peregrinus (for IEE), 1984.
4. A.D. Olver, P.J.B. Clarricoats, A.A. Kishk and L. Shafai, *Microwave Horns and Feeds,* IEEE Press, 1994.
5. S. Ramo, J.R. Whinnery and T. van Duzer, *Fields and Waves in Communication Electronics*, 2nd Edition, Wiley, 1984.
6. S.E. Church et al, "A compact high-efficiency feed structure for cosmic microwave background astronomy at millimetre wavelengths," *30th ESLAB Symposium on Submm and Far-IR Space Instrumentation*, ESTEC, Nordwijk, the Netherlands. 1996
7. B. Maffei, et. al."Corrugated Gaussian Back-to-Back horns for Cosmic Microwave Background continuum receivers," *IEE Antenna Symposium 2000*, QMW, London. April 2000.